Prediction of Unsteady Pressure and Velocity over a Rotorcraft in Forward Flight

N. M. Komerath,* D. M. Mavris,† and S. G. Liou†
Georgia Institute of Technology, Atlanta, Georgia 30332

The problem of predicting the periodic three-dimensional vortex-dominated flowfield around a rotorcraft in low-speed forward flight is studied using potential-flow methods, whose results are compared with surface pressure measurements and flow velocity measurements. The test case used is a two-bladed teetering rotor above a hemisphere-cylinder airframe in a wind tunnel. The dominant features of this problem are modeled by a lifting-line/lifting-surface rotor model with a free wake distorting in the presence of the airframe. The airframe flowfield is modeled using a source/doublet panel method. The instantaneous flowfield is computed at specified intervals of rotor azimuth, with the unsteady effects of blade motion added to the formulation. As a simpler alternative, modeling the energy addition at the rotor using actuator segments led to successful prediction of the time-averaged pressure field and the periodic velocity variations along the spine of the airframe. When a fully unsteady potential formulation is used, however, large differences appear between measured and computed periodic velocity at the sides of the airframe. These are due to inadequate understanding of interaction of the rotor tip vortices with the airframe surface. When measured velocity data are used in the vortex interaction region, the surface pressure is predicted quite well, even at the sides.

Nomenclature

CP_u = difference between instantaneous and local mean static pressures, normalized by the tunnel dynamic pressure
R = rotor radius, m
U_∞ = tunnel freestream velocity in m/s
u = velocity component along the tunnel axis, m/s; positive going downstream
v = vertical velocity component, m/s; positive down
X = longitudinal distance from rotor hub center
Xb = longitudinal distance from the airframe nose
Yb = lateral distance from the cylinder axis
Zb = vertical distance from the cylinder axis; positive upward
Z' = vertical distance from the top surface
Ψ = azimuthal location of the ¼-chord line of the reference rotor blade deg; zero at the trailing edge of the rotor disk
Θ = azimuth angle going around the periphery of the cylinder, deg; zero at the top
μ = ratio of freestream velocity to rotor tip speed

Introduction

THE flowfield around a rotorcraft poses a strong challenge to aerodynamicists. The wake and the proximity of the rotor blades cause large effects on the airframe and other components, which in turn modify the operating characteristics of the rotor system. This interactive flowfield is inherently unsteady and contains steep gradients in velocity and pressure, strong vortices, large amplitudes of fluctuation, and unsteady flow reversal. The resulting complexities strain the capabilities of computational and experimental methods.

Presented as Paper 89-1844 at the AIAA 20th Fluid Dynamics, Plasma Dynamics, and Lasers Conference, Buffalo, NY, June 12-14, 1989; received Oct. 27, 1989; revision received July 15, 1990; accepted for publication Aug. 26, 1990.

*Associate Professor, School of Aerospace Engineering. Member AIAA.
†Post-Doctoral Fellow, School of Aerospace Engineering. Member AIAA.

Present prediction methods for complete rotorcraft must depend on approximate representations and modeling, because the computational requirements of more precise methods are as yet far too large. Such methods must be developed in close interaction with experiments. This paper reports on such an effort. A prediction code of relatively modest computational requirements has been synthesized using existing potential-flow methods and has been modified to handle the rotor-airframe interaction problem. A simple geometric configuration has been used to acquire a multifaceted data base on the time-averaged and periodic features of the surface pressure and velocity fields. The interaction occurs through the flowfield; thus, the ability to predict the velocity field is crucial. Validation of this capability requires accurate measurement of the time-varying velocity field, in addition to surface pressure data and flow visualization. This is the other aspect discussed.

Previous Work

Calculation of the velocity field has been of interest to rotary wing aerodynamicists for a long time. Since the wake is dominated by strong tip vortices, the velocity field can be considered to be "induced" by the vortex system and can be calculated using the Biot-Savart law. When calculating rotor loads, the criterion for success is typically the accuracy of prediction of the blade surface pressure distribution. The geometry that gives an accurate blade load distribution is not necessarily the real wake geometry. The distorted wake can be modeled as "prescribed" or "free." In the prescribed wake technique, the wake geometry is specified using an extensive data base.[1] The more general method is to compute the wake geometry iteratively until it is force free.[2] The issue of whether this geometry is indeed the correct one must be resolved by experimental validation. The presence of a fuselage complicates the computation of the wake geometry.

The capability to make detailed comparisons of induced velocities with experimental data is relatively new. The present authors have compared their measurements of near-field velocities of a single rotor blade in hover with a lifting-surface/free-wake calculation[3] and with unsteady Navier-Stokes calculations near the tip of a rotor in hover.[4] Elliott et al.[5] compared free-wake predictions against their experimental data for inflow to a rotor in forward flight. The time-

averaged velocity field of a two-bladed rotor in forward flight was reported in Ref. 6, and measurements of the velocity field of a cylindrical airframe in the wake of the rotor were reported in Ref. 7. The present authors demonstrated successful prediction of the time-averaged surface pressure field of the airframe in the wake of a rotor.[8] In Ref. 8, the energy addition by the rotor was represented by an actuator segment model, so that periodic variations in the velocity field were not accessible. Significant phase shifts were observed between the calculated and measured unsteady pressure fields.[9] Subsequent refinement of the prediction code, as described in detail in the second author's thesis[10] and summarized here, enabled calculation of the periodic variation of velocity and led to a much improved capability for calculating the periodic pressure variation.

Scope and Objectives

The long-term objective of this effort is to understand interaction phenomena and, thus, to develop a comprehensive capability to predict interacting rotorcraft flowfields. The multifaceted data base permits systematic validation of attempts to compute the flowfield from first principles. In this paper, the work of Refs. 8 and 9 is extended to address the issue of predicting the unsteady pressure and velocity fields, and the results are compared with measurements. Results from the formulation, including an unsteady potential, are presented. As the phenomena near the top surface were successfully predicted, the issue became the observed discrepancies on the sides of the airframe, and the limits of the utility of potential-flow models for this problem. This paper is a revised and expanded version of Ref. 11, with further results from Ref. 10 included.

Test Case

Figure 1 shows the rotor-airframe configuration. An extensive set of measurements has been accumulated on the velocity field,[6,7] pressure field,[12] and vortex trajectories.[13] The airframe model is a hemisphere-cylinder of 134-mm diam. The two-bladed rotor, 914 mm in diameter, has two NACA 0015 blades of 86-mm chord rigidly attached to each other and set at 10-deg pitch. The hub teeters about a pin through the rotor shaft, which is tilted forward 6 deg to simulate the forward flight condition. The wind-tunnel test section is 2.74 m wide and 2.31 m high, and it has been shown[14] that tunnel wall effects are negligible for rotor advance ratios above 0.06. This paper presents results obtained at an advance ratio of 0.1 at a tip speed of 2100 rpm.

The rotor thrust was directly measured[15] by attaching the rotor system to a frame mounted on the wind-tunnel balance. Better than 1% accuracy was demonstrated over the range of thrust measurement using static calibration. It was verified that the balance mounting system, no part of which was inside the test section, did not change the steady or periodic airframe surface pressure distributions. The thrust coefficient at μ = 0.1 was 0.00912 with the airframe present as shown in Fig. 1 and was 0.00890 with the airframe removed. The tip path plane orientation is specified by the angles of attack and roll with respect to the freestream, since the two blades are fixed to each other and coning is negligible. These angles are measured[14] for each test condition by moving a laser beam using the laser Doppler velocimeter (LDV) traverse system to within 0.01-deg error. Independent measurement of the tip path orientation and thrust enabled verification of the rotor trim calculation.

Several simplifications are possible. The rotor tip Mach number is too low to cause significant compressible-flow effects. The airframe shape is kept simple for geometric modeling and instrumentation. From the time-averaged results,[12] no flow separation is seen on the airframe, even at the bottom surface. The rotor blades are rigid. The freestream turbulence intensity is under 0.5%, and the flow phenomena repeat quite well from one revolution to the next. The rotor hub has minimal dimensions. Since the rotor is hung from above, there is no rotor mast on the airframe, so that interference with the rotor flowfield is reduced. However, the test case does show strong interaction effects, and the airframe is larger with respect to the rotor than a usual rotorcraft would be.

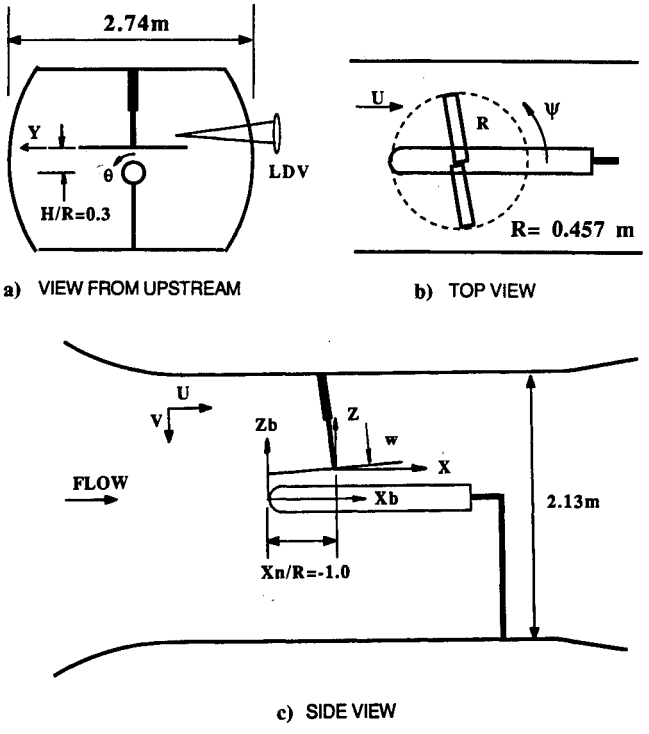

Fig. 1 Rotor-airframe configuration installed in the John J. Harper Wind Tunnel.

Conceptual Model of the Flowfield

Figure 2 shows some of the expected features of the flowfield,[15] with a single rotor blade above the airframe. The only symmetry assumption is that all events repeat every half-revolution, with a two-bladed rotor. The energy added by the rotor increases the stagnation pressure of the flow to levels much higher than that of the freestream. This difference varies with the radial location of passage through the rotor plane, and the azimuth of the rotor at that instant. The envelope of the rotor wake, as defined by the trajectory of the vortex system from the blades, flows over the airframe. The airframe

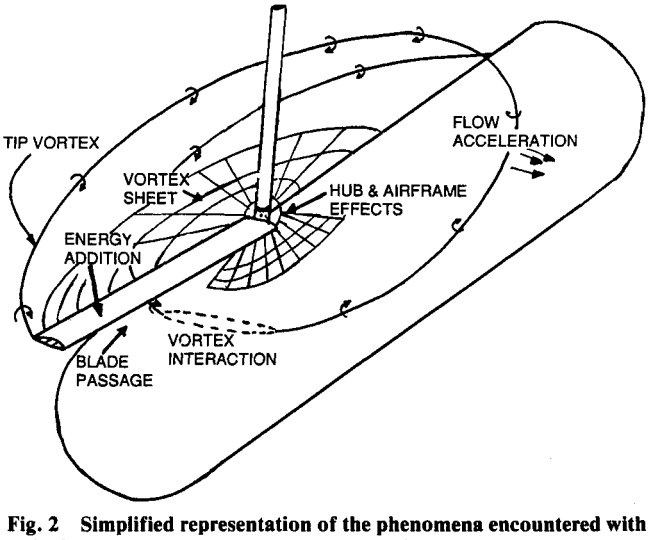

Fig. 2 Simplified representation of the phenomena encountered with a single-bladed rotor and a hemisphere-cylinder.

should, thus, exhibit several features of a yawed cylinder in nonuniform onset flow.

An observer on a rotor blade sees periodic changes in the inflow and the tip airspeed. Forward flight adds asymmetry to the blade flowfield. It skews the wake, sweeping the vortices downstream. Interactions between vortices also distort their trajectories. The presence of the airframe must affect the flowfield at the rotor. An observer on the airframe sees a highly unsteady flowfield. Each passage of a blade causes large pressure and velocity fluctuations. Each approach of a tip vortex filament also causes large changes. The inboard vortex sheets also interact with the airframe. These effects repeat at the blade passage frequency; however, the different features move at different speeds, and their effects may persist on the surface for varying periods.

Instrumentation and Data Base

The different types of data acquired for this test case are summarized in Ref. 15. The time-averaged airframe surface pressure was measured using static pressure taps, and the periodic surface pressure using condenser microphones. Vortex trajectories were documented as functions of rotor azimuth by tracking the motion of vortex core cross sections in planes illuminated by a strobed laser sheet. An LDV was used for flow velocity. A pair of mineral oil atomizers located downstream of the test section enabled uniform seeding of the section with particles in the 5-μ size range. Steady data rates exceeded 1000/s.[14] The data were sorted according to the azimuth of the reference blade at the instant of collection and were ensemble-averaged.

The leading edge of the tip path plane was found to be 4.06 deg below the tunnel longitudinal axis, and the tip of the retreating edge of the plane was 2.02 deg above the lateral axis with the airframe present, as shown in Fig. 1. The corresponding values with the airframe removed were 4.59 and 2.13 deg, respectively. The velocity components chosen were u, postive downstream, and v, positive downward. The third component, directed across the tunnel and along the optical axis, was inaccessible. A detailed set of measurements was acquired near the airframe. Some constraints were encountered. The side under the advancing blade was not optically accessible. At the 90-deg waterline, the measuring point was moved 36 mm from the surface to avoid surface scattering problems.

Error Bounds

Time averages include 30,000 individual measurements from seed particles at each location. The limiting error is the determination of the fringe spacing of the LDV, which is of the order of 1%. In the periodic velocity, each value may represent the average of as few as 20 individual points, especially in azimuth intervals when the vortex core passes. Here the error may be as much as 10%. Unfortunately, these points are also likely to be at extrema of the variations. At other azimuths, each value is the average of about 500 measurements, and the accuracy is again limited by the fringe spacing measurement to 1%.

Prediction Method

The choice of a prediction method was influenced by several factors. The rotor model had to permit nonuniform inflow, and the instantaneous rotor wake geometry had to be accessible. The wake had to distort due to the airframe. The airframe onset flow had to be nonuniform and time varying. Close vortex-surface encounters had to be allowed. Parametric variation runs had to be affordable. Accurate modeling of compressible or viscous effects was not attempted. This, as expected, causes failure to predict the details of vortex-surface interaction phenomena. Thus, Scully's code[2] was selected for the rotor and wake, and VSAERO[16-18] for the airframe. The interface required transformations of reference frames and incorporation of the unsteady effects of relative motion.

Rotor and Wake Modeling

Scully's code implements incompressible lifting-line theory, except in the near field of the rotor, where lifting-surface calculations are used. Steady equilibrium flight is assumed. The wake is represented by a tip vortex with strength varying with vortex age, a vortex sheet from the blade, and a shed wake for azimuthal variations. Different vortex core models are available. Here, two parts of the code for airload and wake geometry computations were merged for operational efficiency.

Airloads are calculated iteratively,[10] as follows: the initial estimate of the bound circulation based on a specified rigid wake geometry is used to calculate the nonuniform inflow to the rotor disk. The angle of attack, aerodynamic loading, and blade motion are calculated. This procedure is repeated to convergence using the new circulation estimate. This requires 5 iterations when 24 azimuthal and 6 radial stations are used. The tip vortex geometry is modified by the new bound circulation, and the induced velocity and aerodynamic loading are recalculated. The procedure is repeated to convergence. The resulting vortex geometry relative to a rotor blade is used to calculate induced velocities.

Airframe Modeling

The airframe surface is discretized using flat, contiguous quadrilateral panels. Program VSAERO reduces the Laplace equation to a set of algebraic equations for surface doublet strengths to satisfy tangential-flow boundary conditions at the panel control points. This system of equations is solved by a blocked Gauss-Seidel procedure. The surface pressure distribution and the flowfield velocities are derived from the singularity strengths. The capability to incorporate wakes using panels was not exercised. This results in failure to conserve vorticity, since the wake of the fuselage is not calculated. The effects of neglecting this have not been studied; indications from the results are that pressures and velocities near the upper surface of the airframe are not seriously affected.

Interaction Scheme

The interface between the rotor and airframe codes requires the consideration of some additional phenomena. Two of these are related to the relative motion between the rotor and airframe, and the third is the interaction of vortices with the airframe surface.

Blade Passage

Initially, results from the code totally missed the observed large-amplitude periodic pressure variations along the top waterline of the airframe. As each blade passed over the airframe, a very large pressure signature occurred on the airframe surface, even outside the boundaries of the wake. This resembled the effects of airfoil motion over the measuring location and was successfully modeled as such. The rotor airfoil was represented by vortex panels on the surface, and the induced velocity was computed at specified planes below the rotor. From the velocities, Bernoulli's equation gave the pressure coefficients, which were transformed from blade-fixed to airframe coordinates. The pressure signature shows the effects of the chordwise load distribution on the airfoil section. This effect dominates the pressure under the outboard portion of the rotor, where loading is strong. Reference 8 showed excellent agreement between the measured and computed pressure at such a point on the airframe. Two peaks were observed for each blade passage; these correspond to the leading edge and trailing edge of the airfoil, respectively. The easiest, and most useful, approach to surface pressure prediction is to add the blade passage effect at desired locations. The effect of the bound circulation of the lifting line must be subtracted at these points to avoid double-counting. This superposition allows use of a lifting-line rotor model in the interaction code and would be unnecessary with a more detailed rotor model.

Energy Addition

Relative motion between the rotor and airframe is manifested in other ways. First, the stagnation pressure of the flow increases substantially through the rotor disk. Second, the stagnation pressure associated with each element of the vortex system will depend on the rotor azimuth and radial position where the element was shed. Third, the vortex elements dissipate and interact. The first effect can be modeled by dividing the rotor disk into "actuator segments," of finite azimuthal and radial resolution, over which the time-averaged stagnation pressure is constant. The wake then resembles a skewed contracting tube bundle that conveys a jet toward the airframe. Reference 8 showed excellent agreement between the predicted stagnation pressure distribution across the wake and Kiel probe data. This enables accurate prediction of the time-averaged pressure and velocity on the surface. Introduction of an unsteady potential permitted calculation and validation of the velocity field at arbitrary points for each step of rotor azimuth. This gives results that are equivalent to the actuator segment for time-averaged calculations on the top of the airframe. Surprisingly, when the unsteady potential was included in the formulation, agreement with experiment became worse at the sides. This is one of the issues investigated here.

Figure 3 depicts a flowchart of the interaction code. VSAERO was modified to allow a nonuniform instantaneous onset flow distribution and, also, accurate computation of offbody velocities at specified points. Scully's code was extended to calculate velocity at arbitrary points. Rotor inflow velocities induced by the airframe are added on while computing the bound circulation along the blade, as a function of rotor azimuth. In reality, this contribution must be recalculated at each step of rotor azimuth for each cycle of the iteration. To reduce computation, it is assumed that the body influence on rotor inflow will not change as the blade itself moves to a different location. For the present configuration, this causes no significant error.

Wake distortion is calculated considering velocities induced at each vortex segment by the bound circulation, other parts of the tip vortex, and the airframe. Airloads and blade motions are found as functions of rotor azimuth. The instantaneous velocities at each surface control point are used to obtain the doublet strengths that satisfy the tangential-flow condition. The unsteady potential due to blade motion is added. The instantaneous airframe pressure field is computed. The procedure is repeated in steps of rotor azimuth for a complete revolution. Finally, the blade passage effect is superposed at desired points on the airframe, with the lifting-line contribution subtracted.

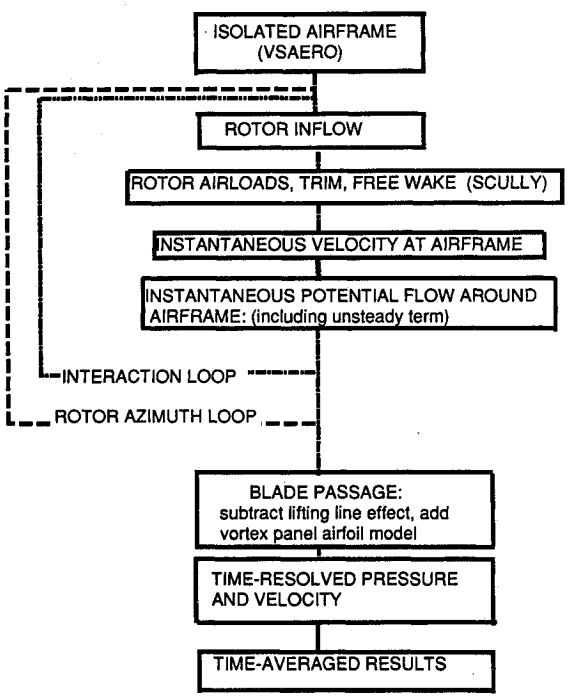

Fig. 3 Flowchart of the computational scheme.

It should be noted that when the unsteady potential is used, the blade passage effect is implicit in the formulation. However, the detailed effects of the chordwise load distribution can be captured only if a detailed blade surface model is used. This was considered unnecessary and expensive here. Thus, the two-dimensional airfoil calculation was performed at surface points where unsteady pressure results were desired, and the lifting-line contribution was subtracted.

Vortex Distortion Around the Airframe

It is possible that the initial rigid vortex geometry specification may include vortex locations inside the volume occupied by the airframe. The following precautions were adopted as conditional procedures in the computational code: 1) an imaginary cylindrical surface was specified around the airframe on which any threatening filaments were forced to stay, and 2) filaments that appeared inside the airframe volume were to be ignored in computing the induced velocity. These conditions have not yet been detected. This is because during iterative computation, the tangency boundary condition forces vortex filaments to distort near the airframe so as to stay off its surface. This procedure is still rather unsatisfactory, since a finite possibility exists that vortex filaments may occur inside the airframe because of the finite steps in azimuth used in computing vortex trajectories.

Results

Mean Velocity Above the Airframe

The time-averaged velocity is obtained by averaging the periodic variation at every location of interest over 24 15-deg intervals of rotor azimuth. To gain a perspective of the results, these distributions are repeated from Ref. 8. Figure 4 shows the two components of velocity along a line located 12.7 mm above the top waterline ($\Theta = 0$).[8] Agreement is excellent over large segments, with v being predicted even better than u. Having thus established that the dominant features of the velocity field can be predicted quite well, the areas of disagreement can be subjected to closer scrutiny. The disagreement is worst where the forward and rear edges of the time-averaged wake interact with the airframe. The u component is underpredicted at the forward edge and overpredicted at the rear edge. Disagreement in v appears to be only in the magnitudes at the extrema.

Going down the sides, the situation deteriorates significantly. Figure 5 shows the comparison at the 60-deg waterline. The comparison points are all 12.7 mm off the surface. Only

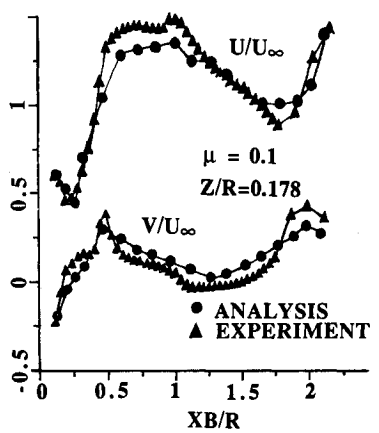

Fig. 4 Time-averaged velocity 12.7 mm above the airframe surface at $\Theta = 0$ deg: a) axial component, b) downward component.

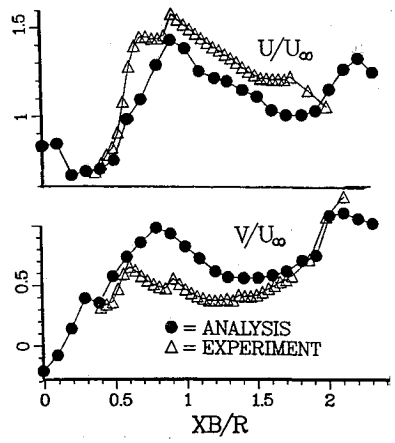

Fig. 5 Time-averaged distribution of velocity at Θ = 60 deg.

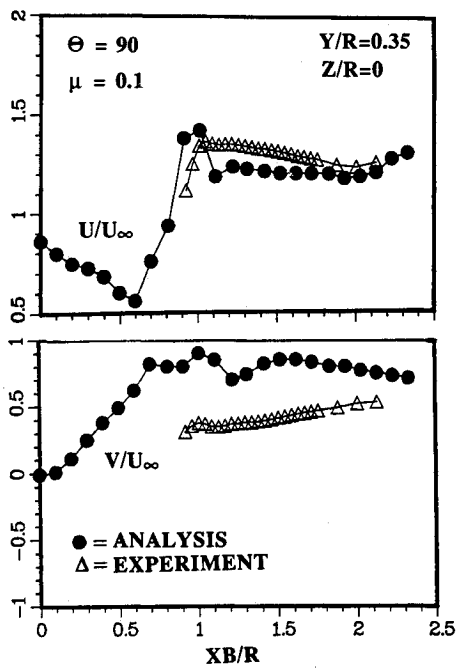

Fig. 6 Time-averaged distribution of velocity along the 90 deg.

the experimental data show a double peak in u near the front edge of the wake. Underprediction of u is now very significant at $XB/R = 0.7$. In this region, v is also very different from the predicted values. At the 90-deg waterline (Fig. 6), agreement has deteriorated further at $XB/R = 0.7$. Along this line, the experimental data for v acquired upstream of $XB/R = 0.7$ had to be discarded.

Periodic Velocity

Figure 7 shows u and v at a point above the top waterline of the airframe and upstream of the wake leading edge. The variations at this location are smooth because the wake does not wash over this point. Agreement is excellent. At $XB/R = 0.37$, the disagreement increases in both velocity components, as shown in Fig. 8. This location is inside the wake, and vortex interaction occurs periodically. Agreement in v is good except for a sharp increase as the vortex impinges on the airframe, whereas u agrees well in amplitudes, but the phase shift indicates that the convective velocity of the features near the surface is in error. The major difference occurs when the tip vortex interacts with the surface. At approximately 200 deg, u drops sharply and even reverses. The boundary layer must have separated upstream. The velocity variation during vortex

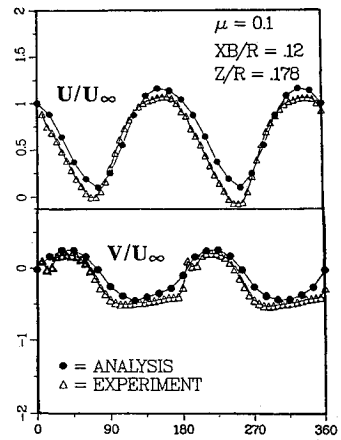

Fig. 7 Periodic variation of velocity at $XB/R = 0.12$.

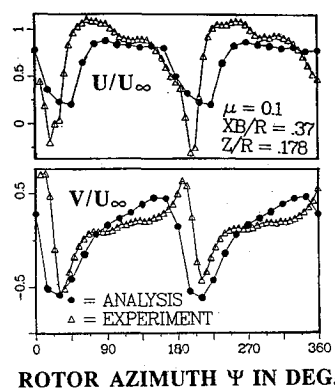

Fig. 8 Periodic variation of velocity at $XB/R = 0.37$.

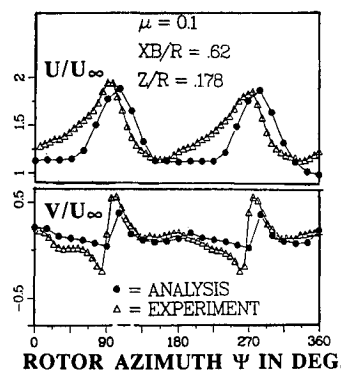

Fig. 9 Periodic variation of velocity at $XB/R = 0.62$.

interaction is quite different from what is calculated, for both components.

At $XB/R = 0.62$, agreement is again quite good, as shown in Fig. 9. This location is still inside the wake, but no vortex interaction occurs here. There is still some disagreement in the secondary features, but the amplitude and phase of the peaks are predicted accurately. Differences become more pronounced again where the aft edge of the wake is felt (not shown). Going farther downstream, Fig. 10 shows that at $XB/R = 2.13$, which is outside the wake impingement region, the predictions match the data again. Substantial fluctuations in velocity still persist in this region. Comparisons at different stations along the 60-deg and 90-deg waterlines are shown in Figs. 11 and 12. As expected from the comparisons of time-averaged velocity, large differences in magnitude appear after the vortex interaction.

Prediction of Unsteady Pressure

Figure 13 compares the measured and predicted instantaneous pressure at three points inside the wake along the top waterline. The most difficult point here is at $XB/R = 0.62$, which is aft of the region of vortex impingement. The agreement here is reasonably good. At $XB/R = 1.2$, the agreement in the amplitude and the phase of the pressure is greatly improved from the corresponding result presented in Ref. 9, where it was calculated using the actuator segment approach. The large-amplitude variations at $XB/R = 1.7$ are captured quite faithfully. Figure 14 examines the pressure prediction on the sides in the region of vortex impingement, at $XB/R = 0.62$ and 1.2. Here, major problems are encountered in predicting the amplitude. The amplitude of the vortex-induced pressure variations is significantly overpredicted; the interaction between the vortex and the airframe cannot be properly accounted for. The problems are worse at $XB/R = 1.2$. The predictions match expectations for a yawed cylinder: flow accelerates over the sides, with the pressure decreasing. The data do not match these at all: the pressure increases down the side of the airframe, and the velocity decreases. This led to examination of whether flow separation was to be expected, based on the crossflow velocity. The lateral component of velocity was not accessible for measurement. The computed time-averaged crossflow velocity vectors over the cylinder at a station near the front edge of wake impingement showed that the crossflow is directed downward, from the retreating blade side to the advancing blade side of the cylinder. Thus, if the airframe is considered to be a cylinder in crossflow, the retreating blade side of the airframe, where the velocity measurements are made, is on the windward side of the airframe on a time-averaged basis. Thus, flow separation need not be feared at 60 deg and 90 deg, and the downward velocities at these locations should be higher than that at the top. The predictions show these trends; the measurements do not. The surface pressure data showed the same disagreement in flow models. Thus, the phenomena on the sides of the cylinder are different from those expected from the potential-flow formulation. One area of insufficient modeling is the vortex-airframe interaction.

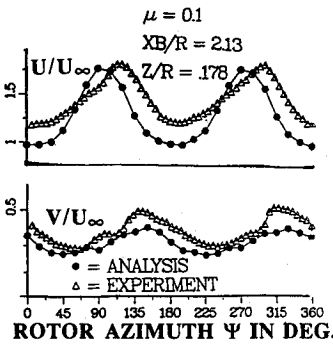

Fig. 10 Periodic variation of velocity at $XB/R = 2.13$.

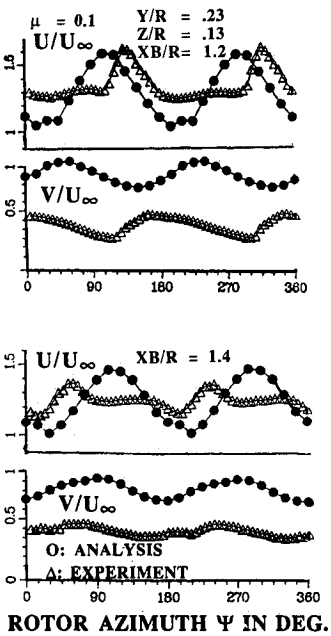

Fig. 11 Periodic variation of velocity at several stations at $\Theta = 60$ deg.

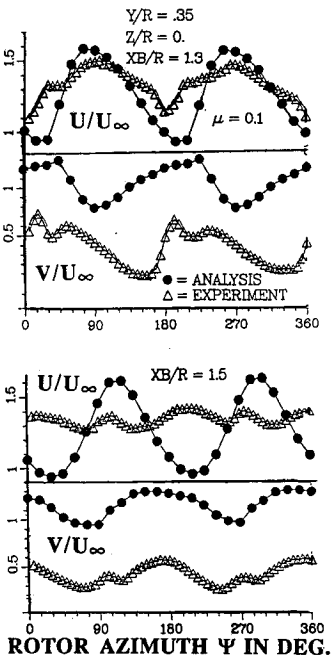

Fig. 12 Periodic variation of velocity at several stations at $\Theta = 90$ deg.

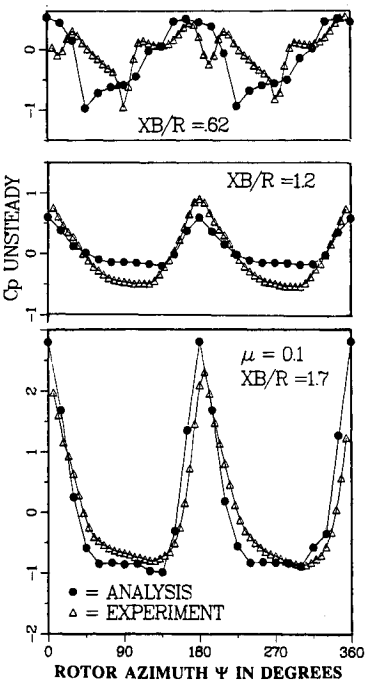

Fig. 13 Periodic variation of surface pressure at three points along the top of the airframe.

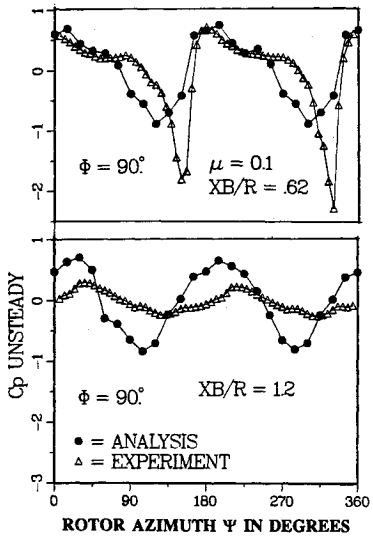

Fig. 14 Periodic variation of surface pressure at two points on the side of the airframe at Θ = 90 deg.

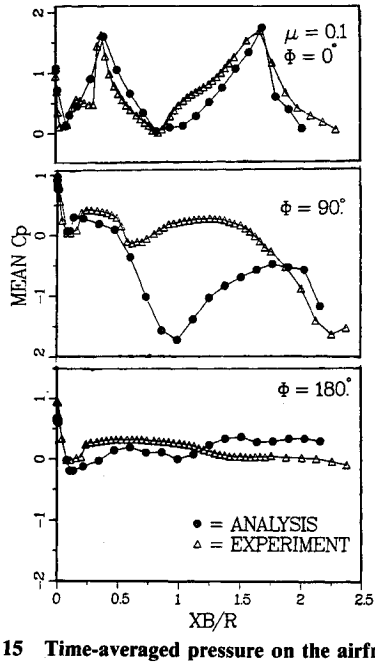

Fig. 15 Time-averaged pressure on the airframe.

Vortex-Airframe Interaction Phenomena

Reference 13 examined the velocity field during interaction of the tip vortex and airframe along the top waterline. The velocity was measured above the top waterline at several instants of rotor azimuth during vortex interaction. The tip vortex was seen to sink into the surface, while a secondary profile formed overhead. This profile appeared downstream of the primary and was convected rapidly. The remaining vortex profile on the sides of the airframe was quite weak and could no longer be seen by flow visualization.[14] Obviously, the induced velocities must also be considerably altered. These phenomena are discussed in more detail in Ref. 12, and further detailed measurements are presented in Refs. 19 and 20; as yet no method is available for their proper modeling.

Effect of Vortex Destruction

The velocity variations along the side suggested that a clue to the disagreement lies in the disappearance of the vortex filaments from the flow visualization after interaction with the cylinder. This was checked by neglecting the contribution of the filaments below Θ = 90 deg. This improved the correlation slightly.

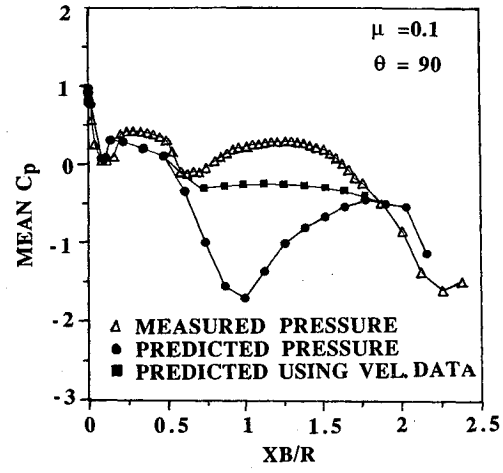

Fig. 16 Effect of using measured velocities to compute the surface pressure variation.

Computation of Time-Averaged Pressure

As realized early in this research program, successful computation of the time-averaged pressure field requires proper inclusion of the large effects of the various unsteady features. Results from the actuator disk approach for the top and sides of the airframe were presented in Refs. 8 and 9. The fully unsteady formulation used here enables calculation of the average pressure all around the airframe. The new results are shown in Fig. 15. Even the sharp peaks of the distribution along the top surface are captured very well. The agreement on the bottom confirms the earlier observation that there is no flow separation on the bottom. There is, however, a large remaining discrepancy on the side.

Pressure Prediction Using Measured Velocity Field

One question is whether knowledge of the correct velocity variation would enable accurate computation of the pressure variation. This was answered by using the *measured* periodic velocity variation in the pressure computation. Unfortunately, as mentioned before, the velocity measurements could not be conducted at the surface but instead had to be 38 mm off the surface at the 90-deg waterline to avoid surface scattering noise. These data were used in the surface pressure computation routine, as an approximate check. The results are compared in Fig. 16 with those computed without empirical input, as well as with measured surface pressure. Use of the measured velocity data, even with the approximations mentioned, results in a very significant improvement in the pressure computation. This further reinforces the conclusion that it is the change in the induced velocity field due to vortex interaction that is missing from the present formulation.

Conclusions

Predictions made using a potential-flow/lifting-line/free-wake computation have been compared to measured results for the velocity field of a hemisphere-cylinder in the wake of a rotor in forward flight. Several conclusions may be drawn.

1) The dominant features of the test case are predicted well on a time-averaged basis along the top and bottom surfaces of the airframe.

2) The periodic variation of velocity above the top waterline is predicted well, except during vortex interaction with the airframe.

3) When rotor energy addition is modeled by time-averaged actuator segments, the mean velocity along the sides is predicted adequately. However, when an unsteady potential is

used, large discrepancies appear in the periodic velocity variation at the side.

4) The effects of vortex impingement are underpredicted. Vortex convection due to the presence of the airframe is underestimated. The multiple peaks in the velocity variation during vortex breakup are not predicted.

5) The observed decrease in velocity on the side of the airframe under the retreating blade is contrary to the prediction, based on potential flow, of flow acceleration around the airframe. The reason for disagreement lies in the phenomenon of vortex-surface interaction.

6) Use of the measured velocity variation near the surface results in greatly improved computation of the surface pressure at the side of the cylinder.

Acknowledgments

This work was supported by the Army Research Office under DAAL03-88-0070-AD2, Aerodynamics Task 2 of the C.E.R.W.A.T. The technical monitor is T. L. Doligalski. Guidance from H. M. McMahon as well as Albert Brand's provision of the surface pressure data are also gratefully acknowledged.

References

[1]Landgrebe, A. J., "An Analytical and Experimental Investigation of Helicopter Rotor Hover Performance and Wake Geometry Characteristics," U.S. Army Aeromechanics Research and Development Lab., USAAMRDL TR71-24, March 1971.

[2]Scully, M. P., "Computation of Helicopter Rotor Wake Geometry and Its Influence on Rotor Harmonic Airloads," ASRLTR 178-1, Massachusetts Inst. of Technology, Cambridge, MA, June 1975.

[3]Komerath, N. M., Thompson, T. L., Kwon, O. J., and Gray, R. B., "The Velocity Field of a Lifting Model Rotor Blade in Hover," *Journal of Aircraft,* Vol. 25, No. 3, 1988, pp. 250–257.

[4]Sankar, N. L., and Komerath, N. M., "Measurement and Computation of the Flow Around the Tip of a Lifting Rotor Blade in Hover," AIAA Paper 88-0047, Jan. 1988.

[5]Elliott, J. W., Althoff, S. L., Sellers, W. L., and Nichols, C. E., "Inflow Velocity Measurements Made on a Helicopter Rotor Using a Two-Component Laser Velocimeter," AIAA Paper 87-1321, June 1987.

[6]Liou, S. G., Komerath, N. M., and McMahon, H. M., "Velocity Measurements of Airframe Effects on a Rotor in Low-Speed Forward Flight," *Journal of Aircraft,* Vol. 26, No. 4, 1989, pp. 340–348.

[7]Liou, S. G., Komerath, N. M., and McMahon, H. M., "The Velocity Field of a Circular Cylinder in the Wake of a Rotor in Forward Flight," *Journal of Aircraft,* Vol. 27, No. 9, 1990, pp. 804–809.

[8]Mavris, D. M., Komerath, N. M., and McMahon, H. M., "Prediction of Rotor/Airframe Aerodynamic Interactions," *Journal of the American Helicopter Society,* Vol. 34, No. 4, 1989, pp. 37–46.

[9]Mavris, D. M., Komerath, N. M., and McMahon, H. M., "Prediction of Unsteady Rotor/Airframe Interactions in Forward Flight," AIAA Paper 88-4420, Aug. 1988.

[10]Mavris, D. M., "An Analytical Method for the Prediction of Unsteady Rotor/Airframe Interactions in Forward Flight," Ph.D. Thesis, Georgia Inst. of Technology, School of Aerospace Engineering, Atlanta, GA, Dec. 1988.

[11]Mavris, D. M., Liou, S. G., Komerath, N. M., and McMahon, H. M., "Prediction and Measurement of the Velocity Field of a Cylinder in the Wake of a Rotor in Forward Flight," AIAA Paper 89-1844, June 1989.

[12]Brand, A. G., McMahon, H. M., and Komerath, N. M., "Surface Pressure Measurements on a Body Subject to Vortex Wake Interaction," *AIAA Journal,* Vol. 27, No. 5, 1989, pp. 569–574.

[13]Brand, A. G., Komerath, N. M., and McMahon, H. M., "Results from the Laser Sheet Visualization of an Incompressible Vortex Wake," *Journal of Aircraft,* Vol. 26, No. 5, 1989, pp. 438–443.

[14]Liou, S. G., "Velocity Measurements on a Lifting Rotor/Airframe Configuration in Low Speed Forward Flight," Ph.D. Thesis, Georgia Inst. of Technology, School of Aerospace Engineering, Atlanta, GA, Dec. 1988.

[15]Komerath, N. M., McMahon, H. M., Brand, A. G., Liou, S. G., and Mavris, D. M., "Measurements and Prediction of the Aerodynamic Interactions Between a Rotor and an Airframe in Forward Flight," *Proceedings of the 45th Annual Forum of the American Helicopter Society,* American Helicopter Society, Washington, DC, May 1989.

[16]Clark, D. R., and Maskew, B., "Study for Prediction of Rotor/Wake/Fuselage Interference, Part 1: Technical Report," NASA CR-177340, March 1985.

[17]Maskew, B., "Program VSAERO, A Computer Program for Calculating the Nonlinear Aerodynamic Characteristics of Arbitrary Configurations," User's Manual, prepared for NASA Ames Research Center, Analytical Methods, Inc., Bellevue, WA, April 1982.

[18]Clark, D. R., and Maskew, B., "Study for Prediction of Rotor/Wake/Fuselage Interference, Part I: Technical Report," NASA CR 177340, March 1985.

[19]Liou, S. G., Komerath, N. M., and McMahon, H. M., "Measurement of the Interaction Between a Rotor Tip Vortex and a Cylinder," *AIAA Journal,* Vol. 28, No. 6, 1990, pp. 975–981.

[20]Brand, A. G., McMahon, H. M., and Komerath, N. M., "Correlation of Rotor Wake/Airframe Interaction Measurements with Flow Visualization Data," *Journal of the American Helicopter Society* (to be published).